

A High-Fidelity Numerical Framework For Wind Farm Simulations

A. Guggeri*, D. Slamovitz*, M. Draper* and G. Usera*
Corresponding author: aguggeri@fing.edu.uy

* Facultad de Ingeniería, Universidad de la República,
Julio Herrera y Reaño 565, Montevideo, Uruguay.

Abstract: A high fidelity numerical framework, based on a LES+ALM approach, to simulate the wind flow through wind farms is presented in this work. The operation of a 7.7MW onshore wind farm was simulated, considering different wind directions and subject to an atmospheric boundary layer (ABL) wind flow, and comparing the results with SCADA (Supervisory Control And Data Acquisition) data of the farm. Good agreement between the electric power and rotor speed mean values is found. Power and velocity deficits due to the wakes of the turbines were well captured in the simulations.

Keywords: Actuator Line Model, LES, Onshore Wind Farm.

1 Introduction

During the last decades, wind energy has seen big technological improvements, related to increases in hub height, rotor diameter and unit power, which has led to larger capacity factors for the same wind speed [1]. Those improvements have supported a rapid expansion all over the world, with annual growth rates of installed capacity around 20%. At present, horizontal axis wind turbines (HAWT) is the technology of greater installed capacity among renewable energies [2].

Recently it took place a significant development of methods and tools for performing high fidelity simulations of wind flows with presence of wind turbines applied to real wind farms. Methods in the frame of Reynolds Averaged Navier-Stokes (RANS) or Large Eddy Simulations (LES) for resolving the wind flow, alongside the Actuator Line Model (ALM) for representing the wind turbines rotors, in which those are represented as body forces. Generally, the strategy followed for simulating a real wind farm under different wind conditions, particularly under different wind directions, has been LES-ADM-R [3] [4], while LES-ALM based methods have been used for evaluating specific wind conditions, particularly one specific wind direction [5] [6] [7]. Based on the precedent, this paper presents an application of the LES-ALM methodology, used for simulating a real wind farm under various wind conditions.

The aim of the present paper is to validate a tool for simulating the operation of a wind farm for numerous wind directions. With that purpose, simulations of the onshore wind farm 'Libertad' were performed. The wind farm consists of 4 wind turbines, Vestas v100, having 2 of them a nominal power of 1950 kW and the remaining 2 a nominal power of 1900 kW. An atmospheric boundary layer (ABL) like inflow condition is considered, along with 14 wind directions, within which, some show strong interactions between the turbines due to their wakes. The `caffa3d.MBRI` solver is used to simulate the wind flow, and the Actuator Line Model (ALM) is used to represent the turbines. The results obtained from the simulations seem acceptable when compared with SCADA data.

The rest of the paper is organized as follows: Section 2 presents a brief description of the numerical solver `caffa3d.MBRI` and the implementation of the ALM, Section 3 describes the wind farm mentioned above, Section 4 describes the simulation setup, Section 5 presents the main results, and conclusions are given in Section 6.

2 Numerical Model

2.1 CFD solver

caffa3d.MBRi [8] [9] is an open source, finite volume (FV) code, second order accurate in space and time, parallelized with MPI, in which the domain is divided in unstructured blocks of structured grids. The mathematical model comprises the mass balance equation (1) and momentum balance equation (2) for a viscous incompressible fluid, together with generic passive scalar transport equation (3) for scalar field ϕ with diffusion coefficient Γ . Note that (2) has been written only for the first Cartesian direction \hat{e}_1 . The balance equations are written for a region Ω , limited by a closed surface S , with outward pointing normal \hat{n}_S .

$$\int_S (\vec{v} \cdot \hat{n}_S) dS = 0 \quad (1)$$

$$\int_{\Omega} \rho \frac{\partial u}{\partial t} d\Omega + \int_S \rho u (\vec{v} \cdot \hat{n}_S) dS = \int_{\Omega} \rho \beta (T - T_{ref}) \vec{g} \cdot \hat{e}_1 d\Omega + \int_S -p \hat{n}_S \cdot \hat{e}_1 dS + \int_S (2\mu D \cdot \hat{n}_S) \cdot \hat{e}_1 dS \quad (2)$$

$$\int_{\Omega} \rho \frac{\partial \phi}{\partial t} d\Omega + \int_S \rho \phi (\vec{v} \cdot \hat{n}_S) dS = \int_S \Gamma (\nabla \phi \cdot \hat{n}_S) dS \quad (3)$$

where $\vec{v} = (u, v, w)$ is the fluid velocity, ρ is the density, β is the thermal expansion factor, T is the fluid temperature and T_{ref} a reference temperature, \vec{g} is the gravity, p is the pressure, μ is the dynamic viscosity of the fluid and D is the strain tensor. The use of equations in their global balance form, together with the finite volume method, as opposed to the differential form, favors enforcing conservation properties for fundamental magnitudes as mass and momentum into the solving procedure [10].

Representation of complex geometries can be handled through a combination of body fitted grids and the immersed boundary method over both Cartesian and body fitted grid blocks. Geometrical properties and flow properties, which are expressed in primitive variables, are always expressed in a Cartesian coordinate system, using a collocated arrangement. Regarding the turbulence model, different subgrid scale models in the context of Large Eddy Simulation (LES) are implemented: the standard Smagorinsky model [11] with damping function for smooth [10] and rough surfaces [12], the dynamic Smagorinsky model [13] with different averaging schemes, the dynamic mixed Smagorinsky model [14] and the scale-dependent dynamic Smagorinsky model [15] with different averaging schemes. Further details of the solver together with validations can be found in [8, 16].

2.2 Actuator Line Model

The ALM has been implemented in the code [17] to represent wind turbines rotors in the simulations.

Each blade is represented as a line that moves with the rotational speed of the rotor and is discretized in radial sections where the aerodynamic forces are computed (Figure 1, left). The geometrical properties of the blades (chord length and twist angle (β)) as well as aerodynamic properties (lift and drag coefficients) are necessary to compute the force in each radial section (Figure 1, right). The former are obtained directly from the wind turbine model, while the aerodynamic coefficients are computed from tabulated data of the corresponding airfoil. At each radial section the aerodynamic force is computed as equation 4.

$$\vec{f} = -\frac{1}{2} \rho V_{rel}^2 c (C_L \vec{e}_L + C_D \vec{e}_D) dr \quad (4)$$

where ρ is the air density, V_{rel} is the relative velocity, c is the chord length, C_L is the lift coefficient, C_D is the drag coefficient, \vec{e}_L is a unit vector in the direction of the lift force, \vec{e}_D is a unit vector in the direction of the drag force and dr is the length of the radial section. Prandtl's tip loss correction factor is applied, as it has shown to improve the results [18].

After computing the aerodynamic forces, it is required to project them onto the computational domain as a body force field. To accomplish this, a smearing Gaussian function is used, taking into account the

distance between each grid cell and radial section, and three smearing parameters, one for each direction (n normal, r radial and t tangential).

$$f(d_n, d_r, d_t) = \frac{1}{\epsilon_n \epsilon_r \epsilon_t \pi^{1.5}} e^{-\left(\frac{d_n}{\epsilon_n}\right)^2} e^{-\left(\frac{d_r}{\epsilon_r}\right)^2} e^{-\left(\frac{d_t}{\epsilon_t}\right)^2} \quad (5)$$

At each time step of the simulation, the resulting aerodynamic torque applied to the rotor shaft (M_{aero}) is computed by integration of the tangential forces along the blades, and the rotational speed is obtained from the rotor second cardinal equation (6).

$$I \frac{d\omega}{dt} = M_{aero} - M_{gen} \Rightarrow \omega = \frac{(M_{aero} - M_{gen})}{I} \Delta t + \omega_{t-1} \quad (6)$$

where M_{gen} is the generator torque, ω is the angular speed of the rotor at the current time step, I is the sum of the rotor, shaft and generator inertia considered at the low-speed side. Δt corresponds to the temporal step and ω_{t-1} accounts for the rotational speed of the previous time step. Finally, the aerodynamic and electric power are calculated as the rotational speed multiplied by the shaft aerodynamic torque and the generator torque, respectively (Eq. 7).

$$P_{aero} = M_{aero} \cdot \omega \quad (7)$$

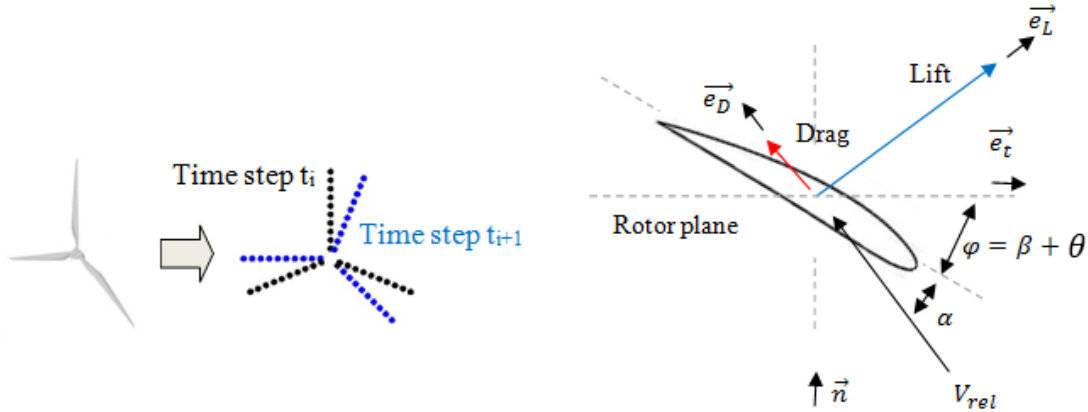


Figure 1: ALM rotor representation (left) and a cross-sectional airfoil radial section (right).

3 Validation case

The simulated wind farm, Libertad, is the same as described in [4]: it is a 7.7MW onshore wind farm located in the south of Uruguay, which has been operating since August 2014 by the Uruguayan company Ventus. It consists of four Vestas V100 wind turbine generators (WT), two with rated power of 1.9MW (WT1 and WT2) and two of 1.95MW (WT3 and WT4), all four with a hub height of 95m and a rotor diameter of 100m. The farm has a meteorological mast (MM) with anemometers at 95m, 80m and 60m, and wind vanes at 93m and 58m height. The wind farm location and layout are shown in Figures 2 and 3.

The terrain surrounding the wind turbines is plane, with no significant slopes according to annex B of IEC 61400-12-1 Standard. Figure 4 shows the wind frequency rose, considering the whole period of operation of the wind farm, almost 4 years, where a predominance of winds coming from the northeast can be observed, which is consistent with the wind farm layout design (see Figure 3).

The data acquired by the SCADA system of the turbines and from the meteorological instruments is compared with the simulations results. The wind turbines data is acquired on a 1 Hz frequency, and recorded on a 10-minute basis, where the mean, standard deviation, maximum and minimum values of more than 250 SCADA signals are available. For this work we consider the 10-minute average of the following 7 signals



Figure 2: Wind farm location



Figure 3: Wind farm layout

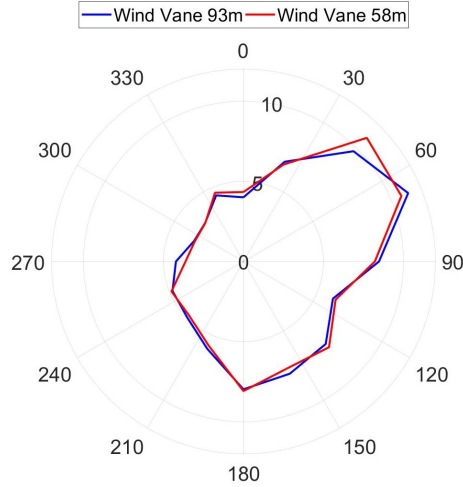


Figure 4: Wind frequency rose

of each turbine: electric power, wind speed, rotor angular speed, blades pitch angle, turbine availability, alarm-code, and active power reference; and from the meteorological instruments, at each mentioned height, we consider the mean values of wind velocity and direction. Table 1 depicts the signals, their source of measurement, symbols and unity. Sub-index $i = 1 : 4$ refers to each wind turbine; sub-index $j = 95, 80, 60$ refers to mast anemometers heights; sub-index $h = 93, 58$ refers to mast wind vane heights. The velocity standard deviation ($\sigma(U)$) is used to compute the turbulence intensity according to equation 8.

$$TI = \sigma(U) / \bar{U} \quad (8)$$

To compare with the simulation results, only the 10-minute periods with normal operation of the wind turbines is taken into account, so the data is filtered according to the following criteria:

- $AA = 0$
- $OK > 595s$
- $P_{Ref} = P_{rated}$
- $\theta < 90^\circ$

Table 1: Signals of WT SCADA and MM instruments

Signal	Source	Symbol	Unity
Electric power	WT_i	P	kW
Wind velocity	WT_i	V_{WT}	m/s
Rotor Angular Speed	WT_i	Ω	RPM
Blade pitch angle	WT_i	θ	$^\circ$
Turbine availability	WT_i	OK	s
Alarm-code	WT_i	AA	non dimensional
Active power reference	WT_i	P_{Ref}	kW
Wind velocity	MM_{Height_j}	V_{MMH_j}	m/s
Wind turbulence intensity	MM_{Height_j}	TI_{MMH_j}	$\%$
Wind direction	MM_{Height_k}	d_{MMH_k}	$^\circ$

Considering the filtered data, Figure 5 depicts a scatter plot of velocity vs power measured at the turbine, together with the manufacturer power curve, for each WT. Still after applying the mentioned filters, a high dispersion of the data can be observed, which can be explained by the following reasons, among others: the natural temporal and spacial variability of the wind, particularly for each direction there is a different terrain influence and turbine-wake interaction; the atmospheric stability, with different wind shear profiles and turbulence intensities, which affect the operation of the WT as well as the characteristics of their wakes; and also other operational aspects of the turbines, such as degradation of their components over time, for example the blades, also contribute to the dispersion of the scatter.

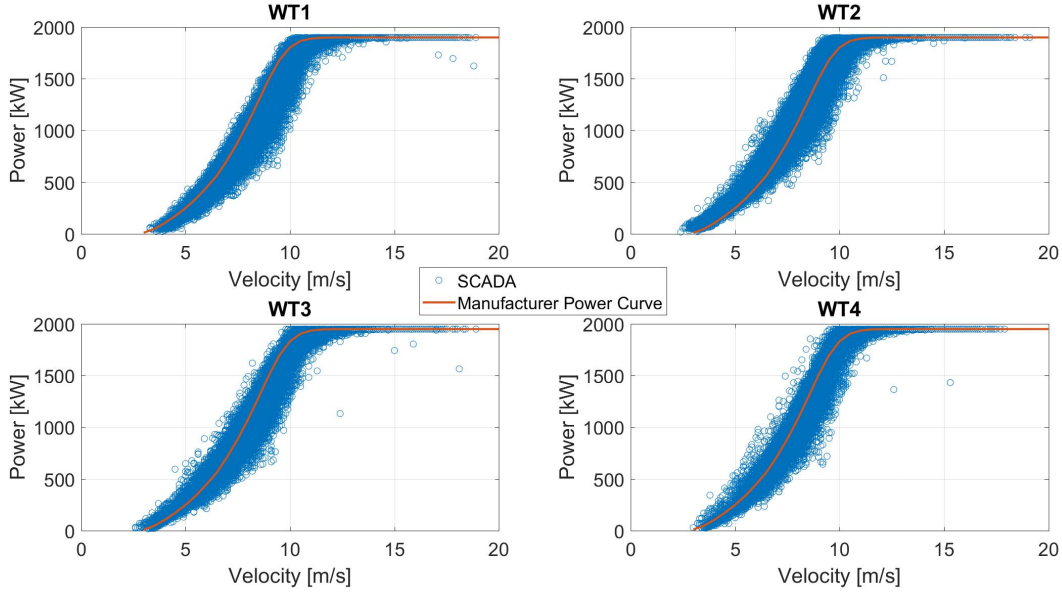


Figure 5: Scatter plot of SCADA velocity vs power manufacturer power curve

For the comparison with the simulation results, additional filters are applied to the SCADA dataset, considering the wind direction measured by the wind vane at 93m, and wind velocity measured by the anemometers at 95m, according to the following criteria:

- $V_{MM_{95}} \in (V_{Ref} \pm 0.25m/s)$
- $d_{MM_{93}} \in (D_{Ref} \pm \Delta d \text{ }^\circ)$

Where V_{Ref} correspond to the wind velocity of the simulation at hub height (95m) and 280 meters upstream of the first WT of on the row. The reason to consider this value rather than the velocity at a fixed position, for example at the meteorological mast is the span-wise variability of the velocity at the inlet, and is further explained in Section 4.2.

$(D_{Ref} \pm \Delta d \text{ }^\circ)$ represents a wind sector: D_{Ref} accounts for the average of two consecutive simulations while Δd is the difference between D_{Ref} and the direction of an individual simulation, in some cases 5° and in others 10° . For example, for simulations 150° and 160° , D_{Ref} is 155° and $\Delta d = 5^\circ$; for simulations 200° and 220° , D_{Ref} is 210° and $\Delta d = 10^\circ$. In order to compute the power and rotor speed associated to each wind sector, averages were computed taking into account the results of the consecutive simulations. No filters considering turbulence intensity or wind shear were applied, as in that case too few data would have fulfilled the criteria. As explained previously in this Section, these atmospheric variables contribute to the dispersion of the power values, as it will be noticed on Section 5. Results.

4 Simulation setup

This Section is divided into three subsections. The first one details the characteristics of the domain, grid, time step, boundary conditions, and wind turbines representation; the second presents the precursor simulation used as inlet boundary condition of the simulations; and the third Subsection describes the axiomatization of the procedure for simulating the operation of the wind farm for numerous wind directions.

4.1 Numerical setup

The size of the computational domain for all the simulations is $3.60\text{km} \times 1.80 \text{ km} \times 0.75 \text{ km}$, the domain is uniformly divided into 288 and 256 cells in the stream-wise and span-wise directions respectively, while in the vertical direction it is divided in 96 cells, which grow up with the distance to the floor with an expansion coefficient of 1.0178. The domain is divided in 16 blocks, which are used for the parallelization with MPI. The inflow condition is obtained from a precursor simulation, while zero velocity gradient is imposed at the outlet and a wall model based on the log law is used to compute the stress at the surface. Periodic conditions are used in the lateral boundaries, and symmetry at the top. The spatial resolution implies a resolution close to $R/4.0$, $R/7.1$, $R/6.5$ in the stream-wise, span-wise and vertical directions respectively; in the vertical direction 23 grid nodes cover the rotor diameter. This grid configuration is the very similar to the thinnest one used in [4]

The Crank-Nicolson scheme is used to advance in time and the scale dependent dynamic Smagorinsky model to compute the subgrid scale stress. To represent the wind turbine rotor the ALM is used the same manner as [4]. The presence of the tower and nacelle are taken into account through drag coefficients, in a similar approach as presented in [19]. The chord and twist angles as well as the airfoil's data, and the relationship between the rotational speed of the rotor and its torque are taken from [4]. Considering the angular velocity of the rotor, the spacial resolution, and previous experiences [4], the temporal step is set at 0.20s.

4.2 Precursor simulation

The precursor simulates an ABL like wind flow, in a domain of the same size and using the same resolution than the domain used for the main simulations, but without considering the topography nor the wind turbines. It is generated considering periodic boundary conditions, with a constant pressure gradient as forcing term, and runs until it reaches statistical convergence. The time evolution of a transversal plane of the precursor is considered as boundary condition at the entrance of the main simulations, as it is usually done for this type of simulations [20] [21] [4].

Figure 6 shows the stream-wise velocity component at the inlet of the simulations, where a significant variation along the span-wise direction can be noticed. This problem has already been observed by the

authors of this paper [4], while in [22] the strategy proposed in [23] is applied to simulate a neutral atmospheric turbulent boundary layer flow with a single turbine and an aligned wind farm, and compared them with a well known experimental campaign. The issue with this span-wise variation is that the velocity at a fixed position of the simulation domain, for example the position of the meteorological mast, may not be representative of the velocity of the whole wind farm when different wind directions are simulated. For this reason, in this work, we consider the reference velocity (V_{Ref}) as the wind velocity of the simulation at hub height (95m) and 280 meters upstream of the first WT of the row. For wind directions between 60° and 240° it is WT4 and for the rest of directions it is WT1. This (V_{Ref}) is used to filter the SCADA data as described in Section 3. It is planned to implement a similar strategy to the one proposed in [23] in the near future, to avoid having a significant span-wise velocity variation at the inlets.

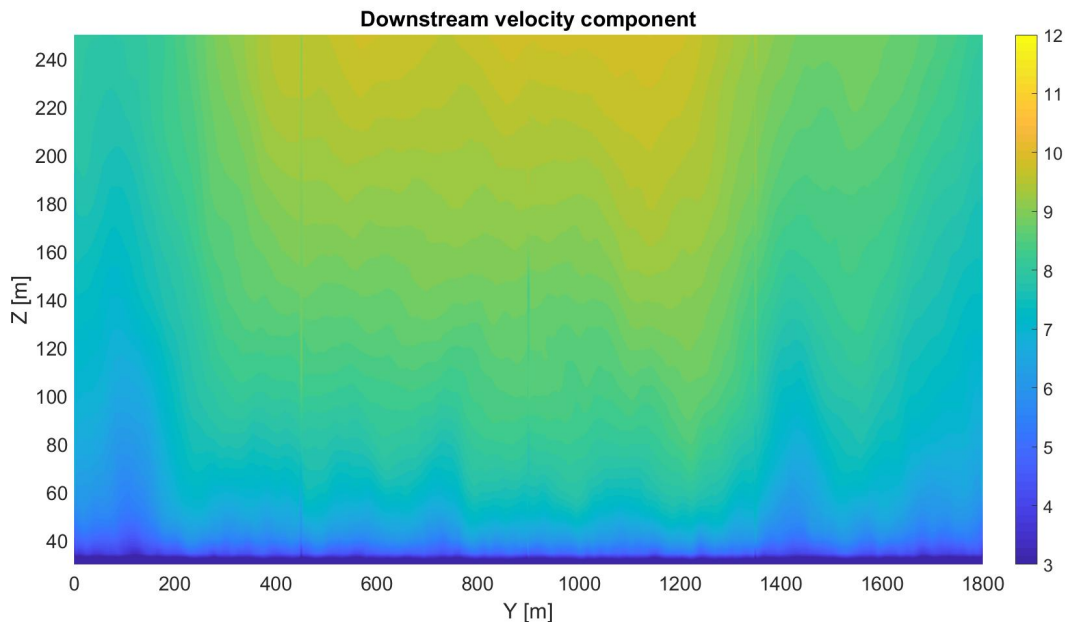


Figure 6: Stream-wise velocity component at the inlet of the simulations

4.3 Automatic grid creation and simulation setup

For simulating numerous directions, the procedure has been automatized, with a Matlab script that has been written and run for this purpose. Some of the inputs for this scripts are the coordinates of the wind turbines and meteorological masts, the height curves around them (e.g in a Computer-Aided Design (CAD) file), the directions aimed to be simulated, alongside other inputs with details of the domain, grid and temporal resolution, wind turbines model, boundary conditions, and computational requisites for the simulation to be run in the computer-cluster. For each direction, the script rotates the domain for making the inlet plane coincide with the west face of the domain. Then it crops the domain according to the given wind direction, domain size and resolution, and it generates all the necessary input files for generating the simulation grid, taking into account the topography and the turbines positions. Those input files are sent to the computer-cluster of Facultad de Ingeniería, where the grid is generated, the simulation is set-up and then begins running, all in an automatic manner. For the wind farm presented in this paper, the procedure until this step takes around 35 minutes, in a 3.6 GHz processor, for each wind direction.

For this wind farm, each simulation requires 16 cores of the cluster (64 GB RAM, Intel(R) Xeon(R) CPU E5-2650 @ 2.00GHz), one for each block. 4000 temporal steps are run, which takes approximately 80 hours, discarding the first 1000 in order to avoid unwanted transitory phenomenons due to sudden appearance of the turbine in the simulations. 3000 temporal steps remain then, which equals to 10 minutes and accounts for 150 turns of the rotor.

Figure 7 illustrates the rotation and cropping of the domain, for direction 150° . At the top left it shows the topography of the domain around the wind farm, with the wind farm location indicated with a red square, at top right it depicts the topography rotated for simulating wind coming from 150° (measured clockwise from the North); then at the bottom the domain used for simulating that direction is shown, where the wind farm topography as well and the wind turbines and meteorological mast positions are shown in better detail.

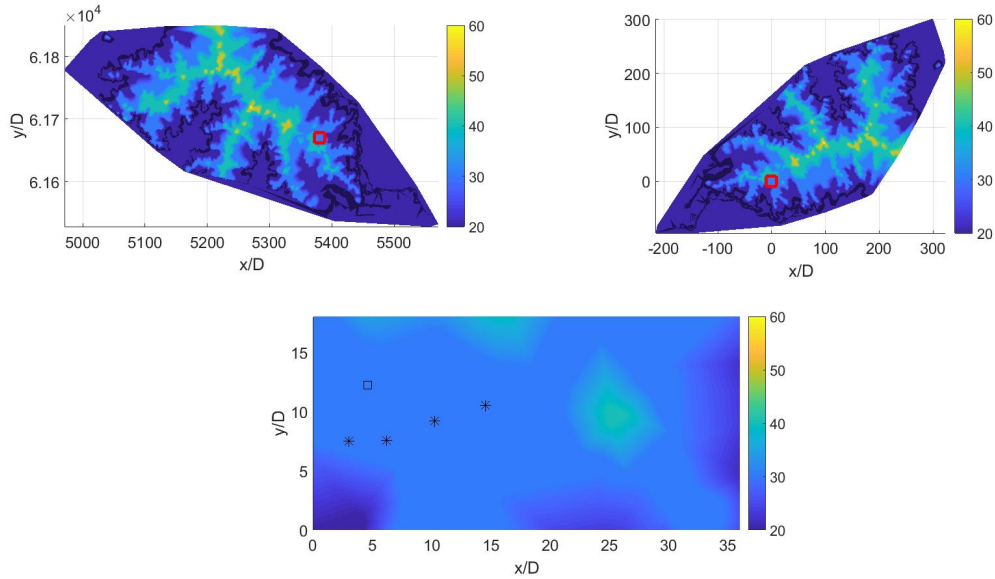


Figure 7: Original domain topography, with the wind farm zone marked in red (up and left), 150° rotated domain topography, with the wind farm zone marked in red (up and right), and 150° rotated and cropped domain topography, with the wind turbines marked with crosses and the meteorological mast marked with a square (down)

5 Results

In this section the results of the wind farm simulations for 14 different wind directions are presented, as described in Section 4, and compared with the data presented in Section 3.

Table 2 depicts the mean values of power and rotor speed, discriminated by wind sector, for each wind turbine and total mean power for the entire farm. The SCADA data is presented as the mean value of datums that fulfill the filters criteria, \pm the standard deviation of those datums. Notice that the standard deviation takes values of the order of hundreds of kW, which is consistent with what is observed in Figure 5. The relative difference between the simulation and SCADA data as well as the standard deviation of the SCADA datasets are also presented. Although significant differences can be observed in some cases, the highest being 57% for WT3 at wind sector $325 \pm 5^\circ$, in all the other cases the simulation averaged value lies between ± 1 standard deviation of SCADA data, both for power and rotor speed. In part, this is due to the high variability of the SCADA data, and because the simulations represent just a particular case among them.

Wind Turbine	Wind sector	D	125	135	145	155	170	190	210	230	305	315	325	335
		DeltaD	5	5	5	5	10	10	10	10	5	5	5	5
WT1	Power [kW]	Simulation	1007	847	1289	1531	1509	1272	1127	1167	1473	1455	1441	1440
		SCADA	1080	840	1063	1368	1374	1619	1298	1363	1180	1144	1471	1624
		SCADA Std	350.1	400.7	423.1	313.2	285.8	305.3	353.1	343.9	325.9	477.8	375.3	318.7
	Rotor Speed [RPM]	Difference	-7%	1%	21%	12%	10%	-21%	-13%	-14%	25%	27%	-2%	-11%
		Simulation	12.8	12.4	14.0	14.5	14.5	14.0	13.6	13.7	14.4	14.4	14.4	14.4
		SCADA	13.4	12.4	13.1	14.2	14.2	14.5	14.0	14.2	14.1	13.9	14.5	14.7
WT2	Power [kW]	Simulation	708	635	1146	1519	1528	1516	1497	1500	1025	769	1197	1467
		SCADA	907	814	1043	1411	1489	1588	1349	1380	1163	820	1130	1648
		SCADA Std	374.6	366.7	427.0	335.8	257.0	296.6	291.3	304.9	353.8	451.9	404.2	332.7
	Rotor Speed [RPM]	Difference	-22%	-22%	10%	8%	3%	-5%	11%	9%	-12%	-6%	6%	-11%
		Simulation	11.8	11.5	13.4	14.5	14.5	14.5	14.5	14.5	12.9	12.1	13.6	14.5
		SCADA	12.5	11.9	12.7	13.9	14.3	14.3	13.7	13.9	13.5	11.8	12.7	14.5
WT3	Power [kW]	Simulation	1507	1139	567	703	1280	1479	1468	1478	835	1001	1453	1499
		SCADA	1264	1203	788	727	1183	1500	1227	1307	775	636	1178	1604
		SCADA Std	295.9	358.6	378.6	357.5	347.0	327.3	334.5	304.1	372.6	289.0	463.1	349.7
	Rotor Speed [RPM]	Difference	19%	-5%	-28%	-3%	8%	-1%	20%	13%	8%	57%	23%	-7%
		Simulation	14.5	13.4	11.0	11.6	13.9	14.5	14.5	14.5	12.4	12.8	14.4	14.5
		SCADA	14.0	13.6	12.2	11.8	13.5	14.2	13.6	14.0	12.3	11.2	13.1	14.5
WT4	Power [kW]	Simulation	1489	1483	1443	1432	1435	1386	1361	1389	1377	939	476	750
		SCADA	1259	1377	1346	1336	1338	1505	1247	1330	1229	860	622	1148
		SCADA Std	284.4	276.1	306.2	294.8	289.2	329.9	340.4	321.9	383.4	493.8	314.6	705.8
	Rotor Speed [RPM]	Difference	18%	8%	7%	7%	7%	-8%	9%	4%	12%	9%	-24%	-35%
		Simulation	14.4	14.4	14.4	14.4	14.4	14.3	14.3	14.3	14.3	12.7	10.7	11.7
		SCADA	13.8	14.0	13.8	13.8	13.8	14.0	13.5	13.7	13.8	12.1	11.4	12.7
Wind Farm	Power [kW]	Simulation	4711	4104	4445	5186	5751	5652	5452	5534	4710	4164	4566	5155
		SCADA	4510	4234	4240	4842	5385	6212	5120	5380	4348	3459	4402	6023
		SCADA Std	1108	1149	1204	1116	1052	1141	1196	1146	1250	1532	1232	1592
	Rotor Speed [RPM]	Difference	4%	-3%	5%	7%	7%	-9%	6%	3%	8%	20%	4%	-14%
		Simulation	14.4	14.4	14.4	14.4	14.4	14.3	14.3	14.3	14.3	12.7	10.7	11.7
		SCADA	13.8	14.0	13.8	13.8	13.8	14.0	13.5	13.7	13.8	12.1	11.4	12.7
Rotor Speed [RPM]	Simulation	14.4	14.4	14.4	14.4	14.4	14.3	14.3	14.3	14.3	12.7	10.7	11.7	
	SCADA	13.8	14.0	13.8	13.8	13.8	14.0	13.5	13.7	13.8	12.1	11.4	12.7	
	SCADA Std	0.83	0.74	0.91	0.75	0.76	0.83	1.02	0.80	1.04	1.86	1.24	2.24	
Rotor Speed [RPM]	Difference	5%	3%	4%	4%	4%	2%	6%	4%	3%	4%	-6%	-8%	
	Simulation	14.4	14.4	14.4	14.4	14.4	14.3	14.3	14.3	14.3	12.7	10.7	11.7	
	SCADA	13.8	14.0	13.8	13.8	13.8	14.0	13.5	13.7	13.8	12.1	11.4	12.7	
Rotor Speed [RPM]	Simulation	14.4	14.4	14.4	14.4	14.4	14.3	14.3	14.3	14.3	12.7	10.7	11.7	
	SCADA	13.8	14.0	13.8	13.8	13.8	14.0	13.5	13.7	13.8	12.1	11.4	12.7	
	SCADA Std	0.83	0.74	0.91	0.75	0.76	0.83	1.02	0.80	1.04	1.86	1.24	2.24	
Rotor Speed [RPM]	Difference	5%	3%	4%	4%	4%	2%	6%	4%	3%	4%	-6%	-8%	
	Simulation	14.4	14.4	14.4	14.4	14.4	14.3	14.3	14.3	14.3	12.7	10.7	11.7	
	SCADA	13.8	14.0	13.8	13.8	13.8	14.0	13.5	13.7	13.8	12.1	11.4	12.7	
Rotor Speed [RPM]	Simulation	14.4	14.4	14.4	14.4	14.4	14.3	14.3	14.3	14.3	12.7	10.7	11.7	
	SCADA	13.8	14.0	13.8	13.8	13.8	14.0	13.5	13.7	13.8	12.1	11.4	12.7	
	SCADA Std	0.83	0.74	0.91	0.75	0.76	0.83	1.02	0.80	1.04	1.86	1.24	2.24	
Rotor Speed [RPM]	Difference	5%	3%	4%	4%	4%	2%	6%	4%	3%	4%	-6%	-8%	
	Simulation	14.4	14.4	14.4	14.4	14.4	14.3	14.3	14.3	14.3	12.7	10.7	11.7	
	SCADA	13.8	14.0	13.8	13.8	13.8	14.0	13.5	13.7	13.8	12.1	11.4	12.7	
Rotor Speed [RPM]	Simulation	14.4	14.4	14.4	14.4	14.4	14.3	14.3	14.3	14.3	12.7	10.7	11.7	
	SCADA	13.8	14.0	13.8	13.8	13.8	14.0	13.5	13.7	13.8	12.1	11.4	12.7	
	SCADA Std	0.83	0.74	0.91	0.75	0.76	0.83	1.02	0.80	1.04	1.86	1.24	2.24	
Rotor Speed [RPM]	Difference	5%	3%	4%	4%	4%	2%	6%	4%	3%	4%	-6%	-8%	
	Simulation	14.4	14.4	14.4	14.4	14.4	14.3	14.3	14.3	14.3	12.7	10.7	11.7	
	SCADA	13.8	14.0	13.8	13.8	13.8	14.0	13.5	13.7	13.8	12.1	11.4	12.7	
Rotor Speed [RPM]	Simulation	14.4	14.4	14.4	14.4	14.4	14.3	14.3	14.3	14.3	12.7	10.7	11.7	
	SCADA	13.8	14.0	13.8	13.8	13.8	14.0	13.5	13.7	13.8	12.1	11.4	12.7	
	SCADA Std	0.83	0.74	0.91	0.75	0.76	0.83	1.02	0.80	1.04	1.86	1.24	2.24	
Rotor Speed [RPM]	Difference	5%	3%	4%	4%	4%	2%	6%	4%	3%	4%	-6%	-8%	
	Simulation	14.4	14.4	14.4	14.4	14.4	14.3	14.3	14.3	14.3	12.7	10.7	11.7	
	SCADA	13.8	14.0	13.8	13.8	13.8	14.0	13.5	13.7	13.8	12.1	11.4	12.7	
Rotor Speed [RPM]	Simulation	14.4	14.4	14.4	14.4	14.4	14.3	14.3	14.3	14.3	12.7	10.7	11.7	
	SCADA	13.8	14.0	13.8	13.8	13.8	14.0	13.5	13.7	13.8	12.1	11.4	12.7	
	SCADA Std	0.83	0.74	0.91	0.75	0.76	0.83	1.02	0.80	1.04	1.86	1.24	2.24	
Rotor Speed [RPM]	Difference	5%	3%	4%	4%	4%	2%	6%	4%	3%	4%	-6%	-8%	
	Simulation	14.4	14.4	14.4	14.4	14.4	14.3	14.3	14.3	14.3	12.7	10.7	11.7	
	SCADA	13.8	14.0	13.8	13.8	13.8	14.0	13.5	13.7	13.8	12.1	11.4	12.7	
Rotor Speed [RPM]	Simulation	14.4	14.4	14.4	14.4	14.4	14.3	14.3	14.3	14.3	12.7	10.7	11.7	
	SCADA	13.8	14.0	13.8	13.8	13.8	14.0	13.5	13.7	13.8	12.1	11.4	12.7	
	SCADA Std	0.83	0.74	0.91	0.75	0.76	0.83	1.02	0.80	1.04	1.86	1.24	2.24	
Rotor Speed [RPM]	Difference	5%	3%	4%	4%	4%	2%	6%	4%	3%	4%	-6%	-8%	
	Simulation	14.4	14.4	14.4	14.4	14.4	14.3	14.3	14.3	14.3	12.7	10.7	11.7	
	SCADA	13.8	14.0	13.8	13.8	13.8	14.0	13.5	13.7	13.8	12.1	11.4	12.7	
Rotor Speed [RPM]	Simulation	14.4	14.4	14.4	14.4	14.4	14.3	14.3	14.3	14.3	12.7	10.7	11.7	
	SCADA	13.8	14.0	13.8	13.8	13.8	14.0	13.5	13.7	13.8	12.1	11.4	12.7	
	SCADA Std	0.83	0.74	0.91	0.75	0.76	0.83	1.02	0.80	1.04	1.86	1.24	2.24	
Rotor Speed [RPM]	Difference	5%	3%	4%	4%	4%	2%	6%	4%	3%	4%	-6%	-8%	
	Simulation	14.4	14.4	14.4	14.4	14.4	14.3	14.3	14.3	14.3	12.7	10.7	11.7	
	SCADA	13.8	14.0	13.8	13.8	13.8	14.0	13.5	13.7	13.8	12.1	11.4	12.7	
Rotor Speed [RPM]	Simulation	14.4	14.4	14.4	14.4	14.4	14.3	14.3	14.3	14.3	12.7	10.7	11.7	
	SCADA	13.8	14.0	13.8	13.8	13.8	14.0	13.5	13.7	13.8	12.1	11.4	12.7	
	SCADA Std	0.83	0.74	0.91	0.75	0.76	0.83	1.02	0.80	1.04	1.86	1.24	2.24	
Rotor Speed [RPM]	Difference	5%	3%	4%	4%	4%	2%	6%	4%	3%	4%	-6%	-8%	
	Simulation	14.4	14.4	14.4	14.4	14.4	14.3	14.3	14.3	14.3	12.7	10.7	11.7	
	SCADA	13.8	14.0	13.8	13.8	13.8	14.0	13.5	13.7	13.8	12.1	11.4	12.7	
Rotor Speed [RPM]	Simulation	14.4	14.4	14.4	14.4	14.4	14.3	14.3	14.3	14.3	12.7	10.7	11.7	
	SCADA	13.8	14.0	13.8	13.8	13.8	14.0	13.5	13.7	13.8	12.1	11.4	12.7	
	SCADA Std	0.83	0.74	0.91	0.75	0.76	0.83	1.02	0.80	1.04	1.86	1.24	2.24	

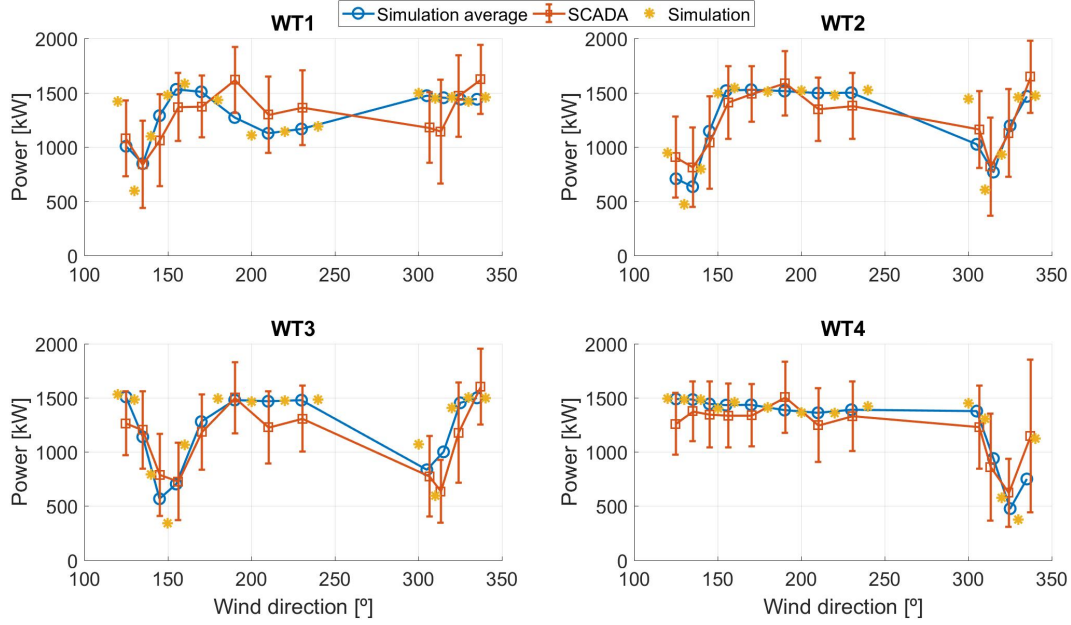


Figure 8: Mean power by direction, simulations vs SCADA data for each wind turbine

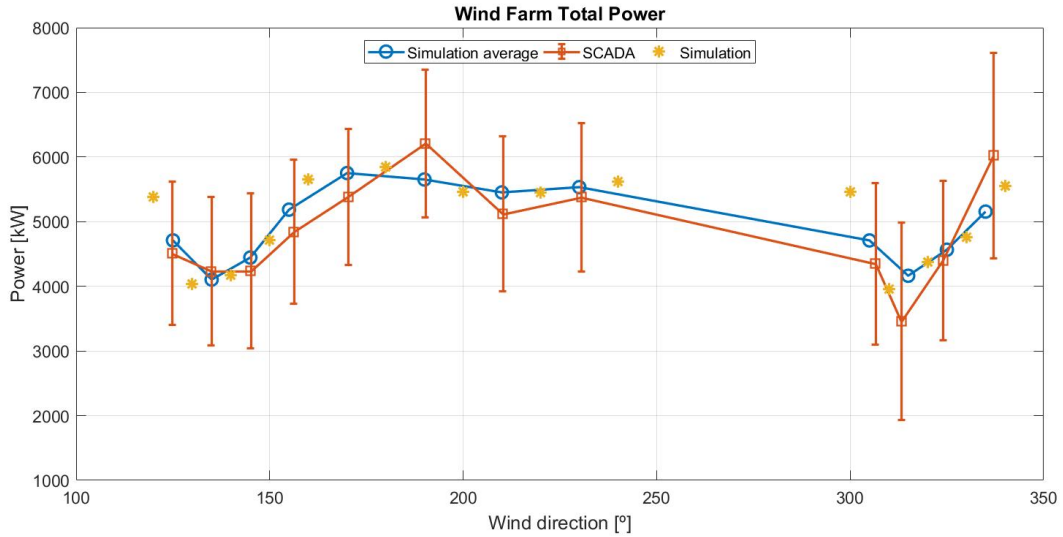


Figure 9: Mean power by direction, simulations vs SCADA data for the whole wind farm

Figure 10 depicts the mean stream-wise velocity on an horizontal plane at hub height, for two directions: 150 ° and 180°. The wakes downstream the rotors can be clearly identified, characterized by a large velocity deficit extending beyond $10D$ downstream. While for the 180° direction, each wind turbine operates without the influence of another WT wake; at 150° the second wind turbine in the row (WT3) is just downstream of WT4, causing its power deficit, as can be seen in Figure 8.

Figure 11 shows the rotor speed of the four WT. Good agreement is found between simulations and SCADA data. When the turbines operate at below rated wind speed, the rotational speed is strongly related to the velocity upstream of the turbine, as it is regulated to operate at the optimal tip speed ratio (TSR) and thus extract the maximum possible power from the wind [24].

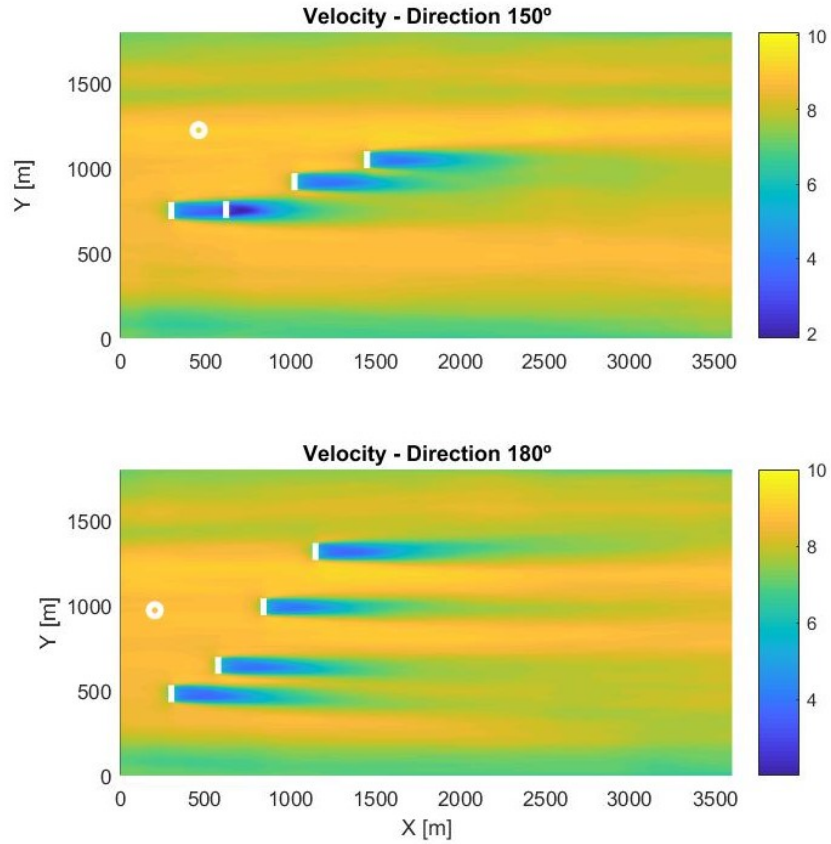


Figure 10: Mean stream-wise velocity, on horizontal plane at hub height, for two directions: Top: 150 ° ; Bottom: 180 ° Wind turbines are represented by white line, and the mast by the white circle

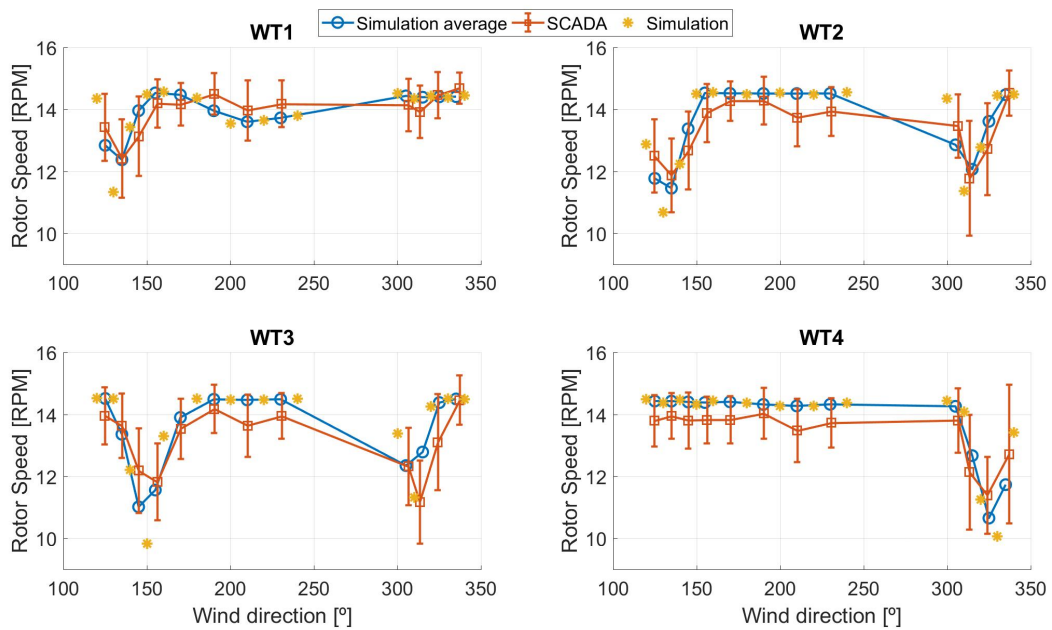


Figure 11: Mean rotor speed by direction, simulations vs SCADA data, for each wind turbine

6 Conclusion and Future Work

A Large Eddy Simulation framework with the Actuator Line Model to represent the wind turbine rotors has been used to simulate the operation of an onshore wind farm considering 14 different wind directions and subject to an ABL wind flow. The electric power and rotor speed simulation results were compared with SCADA data of the farm, finding good agreement between the mean values. Power and velocity deficits were well captured in the simulations.

Future research will focus on the use of this numerical framework to simulate this and other wind farms, considering various ABL profiles as inlet, to evaluate wind resource both at the design and operation stages of wind farms. The use of GPU computing platform as considered in [25] is now being expanded to the full flow solver, using a dual CUDA / OpenCL sintaxis on top of the coarse MPI parallelization. This approach allows achieving speed-ups of up to 30x with respect to the CPU only solver and will be next extended to the wind turbine module routines.

References

- [1] Iea. Technology roadmap - Wind energy. *Technology Roadmap*, page 58, 2013.
- [2] GWEC. Global Wind Report 2015 | Gwec. *Wind energy technology*, page 75, 2016.
- [3] Yu Ting Wu and Fernando Porté-Agel. Modeling turbine wakes and power losses within a wind farm using LES: An application to the Horns Rev offshore wind farm. *Renewable Energy*, 75:945–955, 2015.
- [4] A. Guggeri, M. Draper, and G. Usera. Simulation of a 7.7 MW onshore wind farm with the Actuator Line Model. *Journal of Physics: Conference Series*, 854(1), 2017.
- [5] M. Sessarego, W.Z. Shen, M.P. van der Laan, K.S. Hansen, and W.J. Zhu. CFD simulations of flows in awind farm in complex terrain and comparisons to measurements. *Applied Sciences (Switzerland)*, 8(5):1–21, 2018.
- [6] Fernando Porté-Agel, Yu Ting Wu, Hao Lu, and Robert J. Conzemius. Large-eddy simulation of atmospheric boundary layer flow through wind turbines and wind farms. *Journal of Wind Engineering and Industrial Aerodynamics*, 99(4):154–168, 2011.
- [7] Matthew J Churchfield, Sang Lee, Patrick J Moriarty, Luis A Martinez, Stefano Leonardi, Ganesh Vijayakumar, and James G Brasseur. A large-eddy simulation of wind-plant aerodynamics. *AIAA paper*, 537:2012, 2012.
- [8] G Usera, A Vernet, and J A Ferré. A Parallel Block-Structured Finite Volume Method for Flows in Complex Geometry with Sliding Interfaces. *Flow, Turbulence and Combustion*, 81(3):471, 2008.
- [9] Mariana Mendina, Martin Draper, Ana Paula Kelm Soares, Gabriel Narancio, and Gabriel Usera. A general purpose parallel block structured open source incompressible flow solver. *Cluster Computing*, 17(2):231–241, 2014.
- [10] Joel H Ferziger and Milovan Peric. *Computational Methods for Fluid Dynamics*. Springer-Verlag Berlin Heidelberg, 3 edition, 2002.
- [11] Joseph Smagorinsky. General circulation experiments with the primitive equations: I. The basic experiment. *Monthly weather review*, 91(3):99–164, 1963.
- [12] Paul J Mason and D J Thomson. Stochastic backscatter in large-eddy simulations of boundary layers. *Journal of Fluid Mechanics*, 242:51–78, 1992.
- [13] Massimo Germano, Ugo Piomelli, Parviz Moin, and William H Cabot. A dynamic subgrid-scale eddy viscosity model. *Physics of Fluids A: Fluid Dynamics*, 3(7):1760–1765, 1991.
- [14] Yan Zang, Robert L Street, and Jeffrey R Koseff. A dynamic mixed subgrid-scale model and its application to turbulent recirculating flows. *Physics of Fluids A: Fluid Dynamics*, 5(12):3186–3196, 1993.
- [15] FERNANDO PORTÉ-AGEL, CHARLES MENEVEAU, and MARC B PARLANGE. A scale-dependent dynamic model for large-eddy simulation: application to a neutral atmospheric boundary layer. *Journal of Fluid Mechanics*, 415:261–284, 2000.
- [16] M Mendina, M Draper, A P Kelm Soares, G Narancio, and G Usera. A general purpose parallel block structured open source incompressible flow solver. *Cluster Computing*, 17(2):231–241, nov 2013.
- [17] M Draper. *Simulación del campo de vientos y de la interacción entre aerogeneradores*. PhD thesis, 2015.

- [18] M Draper and G Usera. Evaluation of the Actuator Line Model with coarse resolutions. *Journal of Physics: Conference Series*, 625(1):12021, 2015.
- [19] Yu-Ting Wu and Fernando Porté-Agel. Large-Eddy Simulation of Wind-Turbine Wakes: Evaluation of Turbine Parametrisations. *Boundary-Layer Meteorology*, 138(3):345–366, 2010.
- [20] M Draper, A Guggeri, and G Usera. Modelling one row of Horns Rev wind farm with the Actuator Line Model with coarse resolution. *Journal of Physics: Conference Series*, 753:82028, sep 2016.
- [21] M Draper, A Guggeri, and G Usera. Validation of the Actuator Line Model with coarse resolution in atmospheric sheared and turbulent inflow. *Journal of Physics: Conference Series*, 753:82007, sep 2016.
- [22] R J A M Stevens, L A Martinez-Tossas, and C Meneveau. Comparison of wind farm large eddy simulations using actuator disk and actuator line models with wind tunnel experiments. *Renewable Energy*, 116:470–478, 2018.
- [23] Wim Munters, Charles Meneveau, and Johan Meyers. Shifted periodic boundary conditions for simulations of wall-bounded turbulent flows. *Physics of Fluids*, 28(2), 2016.
- [24] Kurt S. Hansen, Rebecca J. Barthelmie, Leo E. Jensen, and Anders Sommer. The impact of turbulence intensity and atmospheric stability on power deficits due to wind turbine wakes at Horns Rev wind farm. *Wind Energy*.
- [25] Pablo Igounet, Pablo Alfaro, Gabriel Usera, and Pablo Ezzatti. Towards a finite volume model on a many-core platform. *International Journal of High Performance Systems Architecture* 12, 4(2):78–88, 2012.